CrystEngComm

Accepted Manuscript

ROYAL SOCIETY OF CHEMISTRY

www.rsc.org/crystengcomm

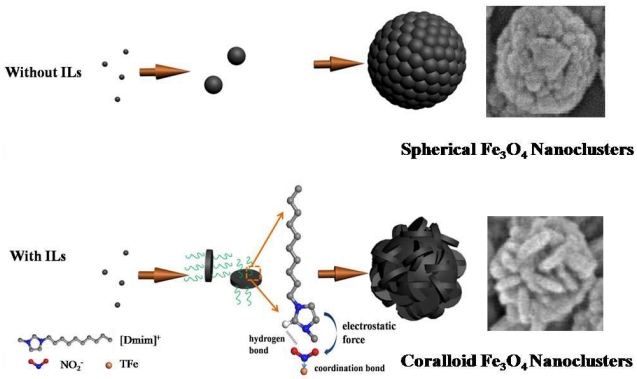

Coralloid Fe_3O_4 nanoclusters stacked by nanosheets, which expose specific plane, have been successfully synthesized with ionic liquid-assisted solvothermal method.

Journal Name

ARTICLE

Controllable synthesis of coralloid Fe_3O_4 nanoclusters in an ionic liquid for catalytic applications

Received 00th January 20xx,
Accepted 00th January 20xx

DOI: 10.1039/x0xx00000x

www.rsc.org/

Kai Sun[a], Changgeng Sun[a], Shaokun Tang[*a,b]

Coralloid Fe_3O_4 nanoclusters stacked by nanosheets are successfully synthesized using ferric nitrate as precursor with ionic liquid-assisted solvothermal method. In comparison, spherical Fe_3O_4 nanoclusters assembled by nanospheres are synthesized in the absence of ILs. The morphologies and structures of the products are further characterized by field emission scanning electron microscopy (FE-SEM), transmission electron microscopy (TEM), X-ray power diffraction (XRD), and X-ray photoelectron spectroscopy (XPS). The results indicate the ionic liquid 1-n-decyl-3-methylimidazolium chloride ([Dmim]Cl) plays an important role in controlling the growth orientation of building blocks via selectively adsorbing on the specific crystal plane. A formation mechanism has been proposed based on the interaction between ILs and Fe_3O_4 crystal planes. The catalytic activity of nanoclusters has been evaluated with the Fention reaction under UVA irradiation. The coralloid nanoclusters show the highest catalytic activity for the degradation of phenol due to the special morphology and unique surface properties. The synthesis strategy may provide a new way to construct nanomaterials with novel morphologies and excellent properties.

Introduction

In recent years, nanostructured magnetic materials have drawn much attention due to their unique properties and extensive applications in biomedical imaging, catalysis, electrochemistry, gas sensors.[1-4] Owing to the significant effects of different nanostructures on magnetic properties, more studies are focused on the controllable synthesis of magnetite with different shapes and sizes.[5-8] Among kinds of synthesis methods such as wet-chemical method,[9] thermal decomposition,[10] chemical vapor depositions (CVDs),[11] solvothermal method has gained more attention due to its innate superiority, especially after Li developed a classic synthesis route.[12] The general method to control and construct the nanostructure of magnetite is by the aid of additives including the specific ions,[13] polymers,[14] organogel[15] or surfactants16 serving as the capping agent or structure-directing agent, which can interact with the specific facets to hinder its growth and the existing large groups can have an effect on the growth of nanocrystals owing to the large steric hindrance.[17] However, in spite of the above exploration, there are few reports on the synthesis of magnetite hierarchical nanostructure with the bottom-up strategy, and how the additives interact with the specific facets still remains pending.

Ionic liquids (ILs), known as green solvents, have been widely applied in many fields based on their outstanding properties such as high thermal stability, excellent solvent properties, and designable structure.[18,19] In the synthesis of inorganic materials, ILs are usually used as template or/and solvent since they can form self-organized structure spontaneously through the electrostatic force, hydrogen bond and π-π stacking, and have strong abilities to dissolve the inorganic precursor resulting from compatible cationic and anionic.[20] ILs are playing a more and more important roles in synthesizing nanomaterials with various morphologies by ionic liquid-assisted solvothermal and ionothermal methods.[21-24] For example, irregular Fe_3O_4 nanoflakes have been synthesized via the solvothermal method assisted by $[C_{16}mim]Cl$ (1-hexadecyl-3-methylimidazolium).[25] However, the shape of products is generally nonuniform and the mechanism of ionic liquid interactions with nanomaterials keeps unclear. Therefore, further investigation is necessary to utilize their excellent properties in fabricating novel inorganic materials.

In this paper, we report a facile and efficient route to synthesize the uniform coralloid Fe_3O_4 nanoclusters by ionic liquids-assisted one step solvothermal method. Furthermore, an ionic liquid induced crystal oriented growth mechanism is proposed for the first time, where the ionic liquid, 1-n-decyl-3-methylimidazolium chloride ([Dmim]Cl), selectively interacts with the specific plane to succeed in morphology control of the synthesized nanoclusters. The degradation of phenol through photo-Fenton reaction was chosen as the model reaction to evaluate the catalytic performance of the as-prepared Fe_3O_4 nanoclusters with novel morphology.

[a] Key Laboratory for Green Chemical Technology of Ministry of Education, School of Chemical Engineering & Technology, Tianjin University, Tianjin 300072, China
[b] Collaborative Innovation Center of Chemical Science and Engineering (Tianjin), Tianjin University, Tianjin 300072, China
E-mail address: shktang@tju.edu.cn

Experimental

Materials

Ferric nitrate ($FeNO_3 \cdot 9H_2O$), ethylene glycol (EG), absolute alcohol, sodium acetate, sodium nitrite, phenol, hydrogen peroxide perchloric acid (analytical grade) were obtained from Tianjin Guangfu Fine Chemical Research Institute. 1-n-decyl-2-methylimidazolium chloride ([Dmim]Cl) was from Lanzhou Greenchem ILS (LICP, CAS, China). Commerical Fe_3O_4 was purchased from Aladdin Industrial Corporation. All the chemicals were used as received without further purification.

Synthesis of coralloid Fe_3O_4 nanoclusters

In a typical procedure, $FeNO_3 \cdot 9H_2O$ (2 mmol) and [Dmim]Cl (2 mmol) were dissolved in 27 mL ethylene glycol to form a homogenous solution with stirring. Subsequently, 12 mmol NaAc was added in the solution. After continuous stirring for 30 min, the mixture was transferred into a Teflon-lined stainless steel autoclave with a capacity of 50 mL for solvothermal treatment at 200 ° C for 24 h and allowed to cool to room temperature naturally. The obtained black precipitates were separated from the solution with an external magnetic field and washed with absolute alcohol and distilled water three times respectively. The final products were dried in vacuum at room temperature for 48 h.

Fe_3O_4-catalyzed Photo-Fenton degradation of phenol

The degradation of phenol was conducted in a beaker under UVA lamp irradiation (8 W) at room temperature. 10 mg Fe_3O_4, 1 mL H_2O_2 (50 mmol/L), and 1 mL phenol solution (5 mmol/L) were mixed in the beaker with stirring. The suspension for irradiation was diluted with deioned water to 50 mL and the pH of the reaction system was adjusted to 3 by the addition of $HClO_4$.

Characterizations

X-ray power diffraction (XRD) analyses were carried out by a Bruker D8 Advance powder X-ray diffractometer with CuKa radiation (λ =1.5418Å). The morphologies were investigated with Hitachi S-4800 field emission scanning electron microscopy (FE-SEM). Transmission electron microscopy (TEM) images and High-resolution TEM (HRTEM) images was taken on JEM-2100F transmission electron microscope (Japan) under a working voltage of 200 KV. The nitrogen adsorption and desorption isotherms at -196oC were measured using an ASAP analyzer (Tristar3000, Micromeritics, USA). XPS analyses of the products were carried out on a Perkin‑Elmer PHI 1600 ESCA system operated at a pass energy of 187.85 eV for survey spectra with an Al Ka X-ray source (E=1486.6 eV). The magnetic property of the sample was measured with a vibrating sample magnetometer (VSM, LDJ 9600-1, USA) at room temperature. The concentration of phenol in the Photo-Fenton reaction was real-time analyzed by high-performance liquid chromatography (HPLC, Regol L-3500) with UV-vis detector. Elution was carried out with a 60:40 mixture of methanol: aqueous at 0.8 mL min−1flow rate with detection at 220 nm.

Results and discussion

Morphology and Structure Characterizations of Fe_3O_4 nanoclusters

Figure 1a and 1b are the typical SEM images of the coralloid Fe_3O_4 nanoclusters with an average diameter of 160 nm synthesized in the presence of [Dmim]Cl. The lower-magnification SEM image (Figure 1b) shows these nanoclusters with uniform size and shape, and the higher-magnification image (Figure 1a) indicates that these nanoclusters are stacking structures of interlaced Fe_3O_4 nanosheets with an average diameter of 40 nm and thickness of 6 nm, resulting in rough surfaces and abundant pores. In comparison, Figure 1c and 1d present the morphologies of Fe_3O_4 synthesized in the absence of ILs. The spherical Fe_3O_4 nanoclusters with a diameter range of 160 nm to 200 nm were constructed by the aggregation of small nanocrystals with approximately 30 nm in size. Since the subunits serving as building blocks have a smaller size and more regular sphere configuration, the surfaces of the obtained spherical nanoclusters are smoother, and meanwhile a number of crevices exist.

The substructures of two kinds of Fe_3O_4 products were further investigated by TEM. The TEM images of the Fe_3O_4 synthesized in the presence of [Dmim]Cl (Figure 2a, 2c) also show the overall coralloid morphology and hierarchical structures with nanosheets. The sizes of the subunits (nanosheets) and nanoclusters are also consistent with the above SEM observations. Figure 2b is the typical TEM images of the Fe_3O_4 synthesized without [Dmim]Cl. It can be clearly observed that the geometrical shape of the nanocluster is sphere with a diameter of 170 nm and the subunits are smaller spherical nanocrystals with a size about 20 nm.

In order to further investigate the growth of the coralloid nanoclusters, HRTEM images of the subunits and their corresponding fast Fourier transform (FFT) patterns are shown in Figure 2d-2f. Figure 2d-2e are the typical HRTEM images of the nanosheets from the top view, the spacings of lattice planes calculated to be 0.253 nm and 0.484 nm, which correspond to the families of crystal planes of Fe_3O_4 respectively. Furthermore, the Fourier transform (FFT) pattern (Figure 2f) was taken to clarify the possible crystal growth orientation and index the exact crystal planes. It is clearly shown that they are both taken along the [01-1] zone axis. The similar result can also been observed from the inset of Figure 2e. These data suggest that the growth of [01-1] direction has been suppressed and the crystal planes can be indexed as (311) and (1-1-1) respectively. As we know, Fe_3O_4 belongs to isometric system. Based on the zone law, we can conclude that the growth of (01-1) plane is hindered. The oriented growth results in the formation of nanosheets subunits instead of the spherical ones with the isotropic growth. It can be speculated that [Dmim]Cl here plays a crucial role in controlling the growth orientation of subunits crystals. This will be discussed deeply later.

XRD analysis was applied to identify the crystal structure and purity of as-prepared samples. Figure 3 shows the XRD patterns of the Fe_3O_4 synthesized in the presence of [Dmim]Cl (a) and in the absence of [Dmim]Cl (b). The relative peak

intensity and position are in good agreement with those of pure Fe_3O_4 with a cubic inverse spinel structure (JCPDS No. 88-0315). There is no extra diffraction peaks, suggesting high purity of the synthesized products. Based on the Debye–Scherrer formula for the strongest (311) diffraction peak, the grain sizes of coralloid Fe_3O_4 nanoclusters and spherical Fe_3O_4 nanoclusters can be respectively calculated as 29.0 and 29.3 nm, indicating that both products are constructed through the assembling of nanocrystal primers. This remains consistent with SEM and TEM observations (Figure 1 and 2). Furthermore, the values calculated from Debye–Scherrer formula reflect the thickness of crystals along the direction perpendicular to the reference crystal plane. In this study, it reflects the thickness along [311] zone axis. The value is comparable with the average diameter of nanosheets subunits, which means [311] zone axis is one of the preferentially growing directions and the crystal growth along [311] will not be hindered, confirming the results from HRTEM and FFT images.

Considering the crystal structure similarity between Fe_3O_4 and γ-Fe_2O_3, it is hard to distinguish them only by XRD analysis.[26] Therefore, X-ray photoelectron spectroscopy (XPS) was further used to investigate the structure and purity of the synthesized nanoclusters. Figure S1 shows the core-level XPS spectrums of the coralloid Fe_3O_4 nanoclusters, two distinct peaks at 712.3 and 726.2 eV are attributed to $Fe2p_{2/3}$ and $Fe2p_{1/2}$, respectively. Remarkably, no satellites can be identified at ~718eV, which matches the characteristics of Fe_3O_4.

Formation Mechanisms of the Coralloid and Spherical Fe_3O_4 Nanoclusetrs

In our experiments, ferric nitrate was chosen as the precursor to replace commonly used ferric chloride. Due to its thermal instability,[27,28] especially in the sealed reductive atmosphere provided by ethylene glycol dehydration at high temperature (200 °C), nitrate (NO_3^-) mainly decomposes into nitrite (NO_2^-),[29] with consumption of the reducing agent (ethylene glycol). The phenomenon has been perceived when we employ ferric nitrate as the precursor following the same reactants molar ratio as Li's method[12] using ferric chloride as the iron source. The products are brown, indicating not pure Fe_3O_4 owing to the extra consumption of the reducing agent during the NO_3^- decomposition.

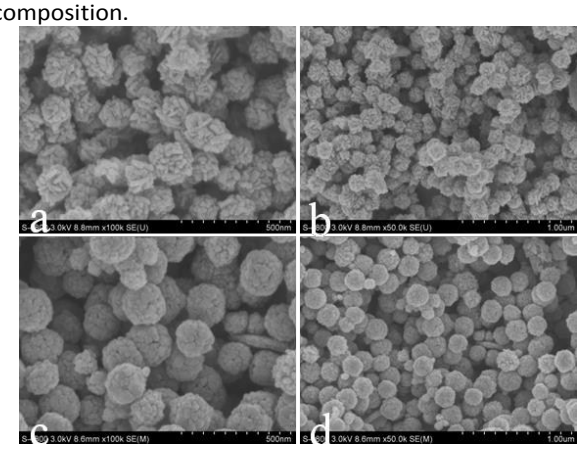

Figure 1. SEM images of coralloid Fe_3O_4 nanoclusters synthesized in the presence of [Dmim]Cl (a, b) and spherical Fe_3O_4 nanoclusters synthesized in the absence of ILs (c, d).

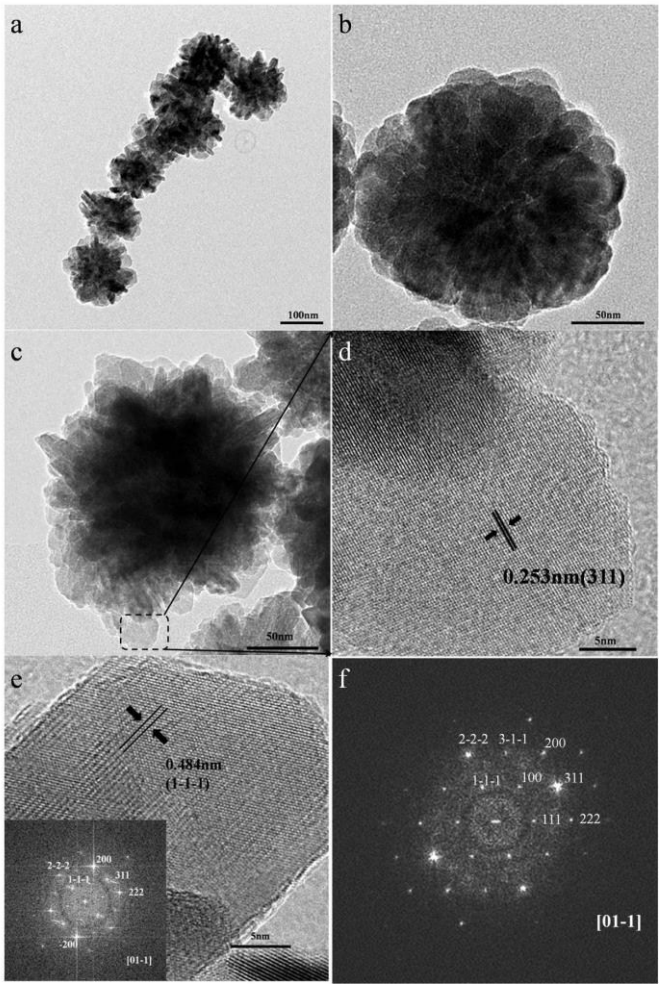

Figure 2. TEM (a,c) and HRTEM (d,e) images of coralloid Fe_3O_4 nanoclusters synthesized in the presence of [Dmim]Cl; b. TEM image of spherical Fe_3O_4 nanoclusters synthesized in the absence of ILs; The inset of (e) is the corresponding FFT pattern; f. FFT pattern of (d); They were both taken along the[01-1] zone axis.

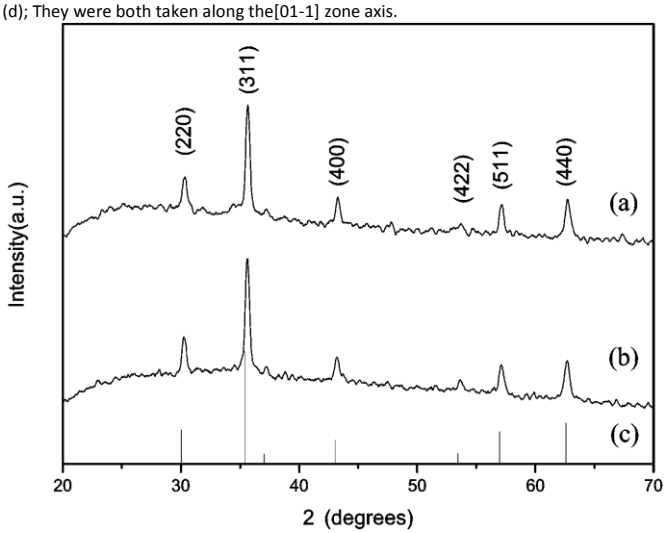

Figure 3. XRD patterns the Fe_3O_4 nanoclusters synthesized: (a) in the presence of [Dmim]Cl and (b) in the absence of [Dmim]Cl; (c) Fe_3O_4, JCPDS card No.88-0315.

As we know, the crystal growth process can be divided into the following three stages: nucleation stage, growth stage and dissolution-recrystalization stage.[21,30] On the lack of stabilizer,

the primary nanocrystals with smaller curvature radius will go through a preferential dissolution process to minimize the surface free energy when the nanocrystals amount increases to a certain level. With the addition of stabilizers, the primary nanocrystals tend to assemble into nanoclusters if the stabilizer concentration is below a certain threshold as the limited ligand protection (LLP) mechanism declares.[31,32] With the further increase of stabilizer concentration to be above the threshold, the primary nanocrystals will not interact with each other and they could stably exist in the solution due to the sterical isolation by the stabilizers; meanwhile, the large amount of the ligands also suffice for protecting them from going through the interparticle Ostwald ripening. In this work, since NO_2^- has stronger coordination ability with transition metal ions than NO_3^-,[33,34] NO_2^- will adsorb on the Fe_3O_4 primary nanocrystals and serve as the stabilizer to control the Fe_3O_4 crystal growth.

To confirm the effect of NO_2^- ion, sodium nitrite was directly added to the reaction system. The TEM image (Figure 4a) shows that the products obtained by adding 4 mmol sodium nitrite in the absence of ILs have smaller size (70 nm) and are composed of fewer primary nanoparticles than spherical nanoclusters (Figure 2b). Moreover, when 8 mmol sodium nitrite was added, the primary nanoparticles could be reasonably stable in solution and will not aggregate into nanolusters as shown in Figure 4b. These results suggest that NO_2^- can serve as the ligand to stabilize the primary nanoparticles efficiently. With the increase of ligand concentration, more and more NO_2^- will adsorb on the nanocrystals to weaken the aggregation and eventually forming monodispersed nanoparticles over the threshold.

On the basis of the above discussion and experiment results, we realize that the major reason for forming Fe_3O_4 nanoclusters with two different types of morphologies (coralloid and spherical) is the different structures of their building blocks (primary nanosheets and nanospheres). Through the analysis of HRTEM and FFT images of coralloid Fe_3O_4 nanoclusters, it is believed that [Dmim]Cl plays a vital role in hindering the growth of (01-1) plane. To investigate the oriented growth mechanism, we cleave the Fe_3O_4 crystal structure and the schematic structures of three typical crystal planes (01-1), (111) and (311) are shown in Scheme 1. the Fe_3O_4 crystal consist of two different Fe atoms: one is located in the central of tetrahedron coordinating with four O atoms (TFe) and the other is in the central of octahedron coordinating with six O atoms (OFe).[35] An interesting phenomenon can be found in Scheme 1. The (01-1) plane, whose growth is suppressed, exposes the OFe, TFe and O atom terminations; in contrast, the facets (111) (311), whose growths are not hindered, only expose OFe terminations. The higher coordination number of Fe (OFe) will increase steric hindrance and electron density, preventing the coordination between NO_2^- and OFe. Therefore, NO_2^- will selectively adsorb on the crystal plane exposing the low coordination number Fe (TFe), viz., it will absorb on the (01-1) plane. However, NO_2^- cannot efficiently suppress the growth of (01-1) due to its small steric hindrance. With the addition of the IL, $[Dmim]^+$ will interact with the NO_2^- through the electrostatic force and the hydrogen-bonding between H atom in C2 position of $[Dmim]^+$ rings and O atom in the NO_2^-.[36] Additionally, the adsorbed $[Dmim]^+$ will form a tight coverage layer on the (01-1) plane by π-π stacking.[22] The triple interactions will anchor the $[Dmim]^+$ on the (01-1) plane firmly and its large steric hindrance will efficiently help preventing the crystal growth along [01-1].

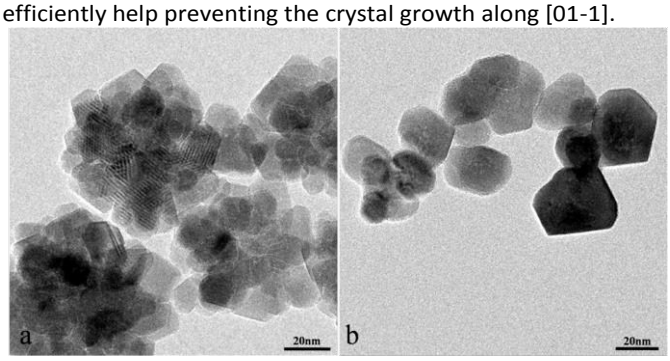

Figure 4. TEM images of synthesized Fe_3O_4 in the absence of [Dmim]Cl with different $NaNO_2$ dosages: (a) 4 mmol, (b) 8 mmol.

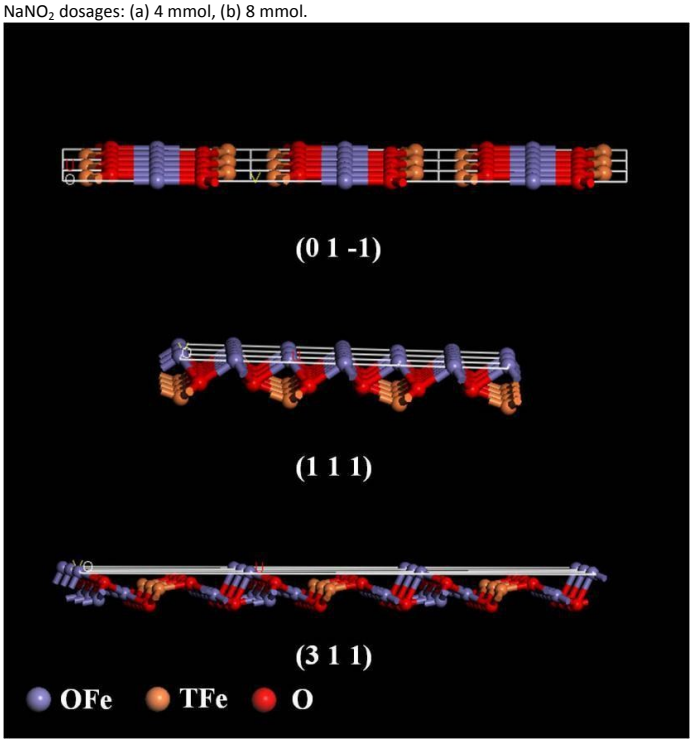

Scheme 1. Schematic structures of three typical Fe_3O_4 crystal planes

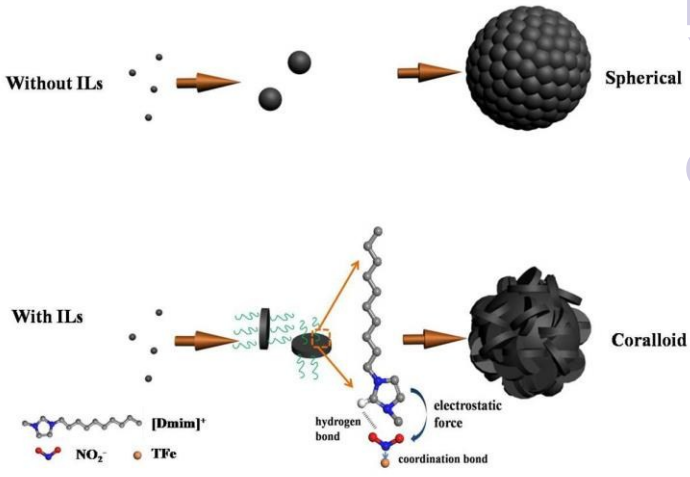

Scheme 2. Schematic illustration of the formation process for the spherical and coralloid Fe_3O_4 nanoclusters

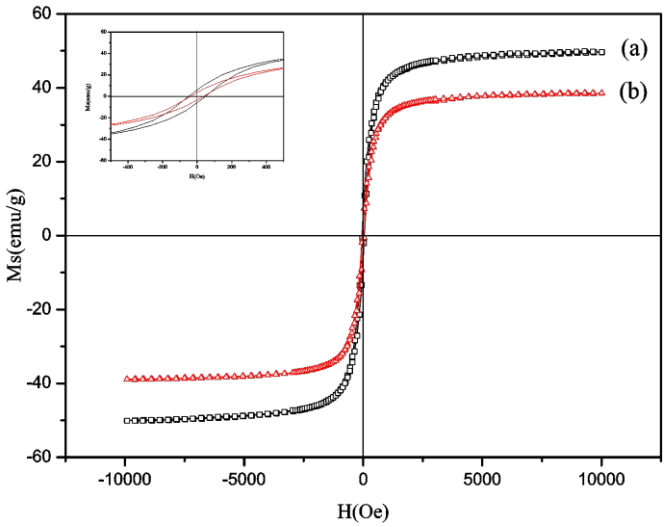

Figure 5. Magnetization hysteresis loops recorded at room temperature of (a) coralloid Fe_3O_4 nanoclusters and (b) spherical Fe_3O_4 nanoclusters. The inset shows the enlarged view of the loops from −500 Oe to +500 Oe region.

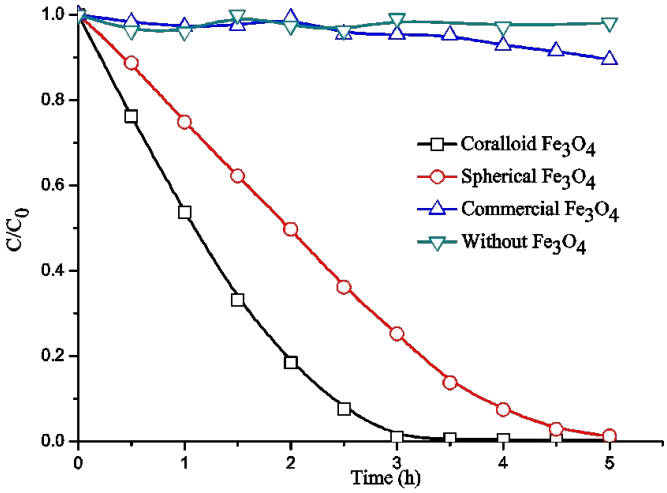

Figure 6. Curves of phenol degradation catalyzed by different Fe_3O_4

For comparison, we conduct the comparative experiment using ferric chloride as the precursor. As shown in Figure S2, the Fe_3O_4 nanoparticles are both compact spherical regardless of whether adding [Dmim]Cl or not, indicating ILs fail to play their role in lack of NO_2^-, It further confirms that the collaboration of NO_2^- and [Dmim]Cl induces the oriented crystalline growth and achieves in the construction of the coralloid nanoclusters. Besides, it also suggests that the coordination bonds between acetic acid radical/ethylene glycol and iron ions are not strong enough for them to serve as stabilizers to induce the formation of nanoclusters structure.

Based on the above discussion, a possible formation mechanism of coralloid and spherical Fe_3O_4 nanoclusters is proposed as shown in Scheme 2. After the classical nucleation stage, the primary nanoparticles are formed through isotropic growth and stabilized by NO_2^- in the absence of [Dmim]Cl; in contrast, primary nanosheets are formed via oriented-growth via the interaction between [Dmim]Cl and NO_2^-. Then, the two types of primary building blocks respectively aggregate into the secondary structures to minimize the total surface free energy, which is thermodynamically favorable, and form their final spherical and coralloid morphologies.

Surface properties and magnetic properties of the Fe_3O_4 Nanoclusters

The specific surface areas of the two kinds of Fe_3O_4 nanoclusters were determined by measuring the nitrogen adsorption and desorption isotherms. The measured BET surface areas of the coralloid and spherical nanoclusters are 23.8m^2g^{-1} and 14.5 m^2g^{-1} respectively, both higher than that of the compact Fe_3O_4 nanoparticles (measured as 10.6 m^2g^{-1}) synthesized with ferric chloride as precursor, indicating the rough surfaces formed through the aggregation of subunits. Notably, the coralloid nanoclusters are composed of oriented growth nanosheets which exposing the (01-1) facet. They may have potential in supporting catalysis to enhance the catalytic activity though the synergy between the exposed specific facet and catalysis[37,38] and their large surface area. Further work is still needed to test the idea. Figure 5 shows the hysteresis loops of the two kinds of Fe_3O_4 nanoclusters. Curve a is for the coralloid Fe_3O_4 and curve b is for the spherical one. It can be found that the saturation magnetization value of the coralloid Fe_3O_4 (50.1 emu·g^{-1}) is higher than that of the spherical Fe_3O_4 (40.2 emu·g^{-1}), which should be attributed to larger size of the primary nanoparticles. However, both of them are lower than that of compact Fe_3O_4 nanoparticles (81.9emu·g^{-1})12 due to more crystal growth defects of the two morphologies.

Photo-Fenton degradation of phenol catalyzed by Fe_3O_4 nanomaterials

To evaluate the performances of the Fe_3O_4 nanoclusters, the as-prepared spherical and coralloid Fe_3O_4 nanoclusters were respectively used as catalysts for photo-Fenton degradation of phenol in this work[37], and commercial Fe_3O_4 nanoparticles were also tested for comparison. Figure 6 shows the curves of phenol concentration vs. time with different Fe_3O_4 as catalysts. It is obvious that the coralloid Fe_3O_4 nanoclusters synthesized with ionic liquids show the highest catalytic activity and the concentration of phenol in the reaction mixture (C) decreases to only 0.0093 of initial concentration of phenol (C_0) in 3 h. Meanwhile, the degradation rate catalyzed by spherical nanoclusters is slower than that with coralloid Fe_3O_4. Moreover, the concentration of phenol has negligible changes even after 5 h when catalyzed by commercial Fe_3O_4 or no catalyst. It can be speculated that the catalytic activity depends on the surface properties of nanomaterials. The commercial Fe_3O_4 has almost no catalytic activity for the reaction due to its monoblock morphology with smooth surface and large particle size (See Figure S3).

Conclusions

In summary, the coralloid Fe_3O_4 nanoclusters with uniform sizes and morphology have been successfully synthesized by a facile and efficient one step ionic liquids-assisted solvothermal method, which exhibits quite different nanostructures compared to the spherical Fe_3O_4 nanoclusters synthesized in the absence ILs. By the aid of the electrostatic interactions and the hydrogen-bonding interaction between $[Dmim]^+$ and NO_2^-, ILs selectively adsorb on the specific (01-1) plane for lower steric hindrance and electron density, control the oriented growth of primary building blocks and construct the final coralloid morphology.

Owing to the excellent properties such as high surface area and exposed specific facet, the coralloid magnetite nanoclusters show the highest catalytic activity in the photo-Fenton degradation of phenol and make them a promising catalyst in water treatment. This synthetic strategy may provide new insights in the applications of ILs for nanomaterials construction with novel morphologies and predominant performances.

Acknowledgements

This project was financially supported by the National Natural Science Foundation of China (21206118, 21328601), the Natural Science Foundation of Tianjin of China (12JCYBJC13500).

Notes and references

1 Daniele, M. A.; Shaughnessy, M. L.; Roeder, R.; Childress, A.; Bandera, Y. P.; Foulger, S., Magnetic Nanoclusters Exhibiting Protein-Activated Near-Infrared Fluorescence. ACS nano 2012, 7, 203-213
2 Deng, Y.; Cai, Y.; Sun, Z.; Liu, J.; Liu, C.; Wei, J.; Li, W.; Liu, C.; Wang, Y.; Zhao, D., Multifunctional mesoporous composite microspheres with well-designed nanostructure: a highly integrated catalyst system. J. Am. Chem. Soc. 2010, 132, 8466-8473.
3 Kang, E.; Jung, Y. S.; Cavanagh, A. S.; Kim, G.-H.; George, S. M.; Dillon, A. C.; Kim, J. K.; Lee, J., Fe_3O_4 Nanoparticles Confined in Mesocellular Carbon Foam for High Performance Anode Materials for Lithium-Ion Batteries. Adv. Funct. Mater. 2011, 21 , 2430-2438.
4 Zhai, Y.; Jin, L.; Wang, P.; Dong, S., Dual-functional Au-Fe_3O_4 dumbbell nanoparticles for sensitive and selective turn-on fluorescent detection of cyanide based on the inner filter effect. Chem. Commun. 2011, 47, 8268-8270.
5 Geng, B.; Zhan, F.; Jiang, H.; Guo, Y.; Xing, Z., Egg albumin as a nanoreactor for growing single-crystalline Fe_3O_4 nanotubes with high yields. Chem. Commun. 2008, 5773-5775.
6 Jia, C. J.; Sun, L. D.; Luo, F.; Han, X. D.; Heyderman, L. J.; Yan, Z. G.; Yan, C. H.; Zheng, K.; Zhang, Z.; Takano, M., Large-scale synthesis of single-crystalline iron oxide magnetic nanorings. J. Am. Chem. Soc. 2008, 130, 16968-16977.
7 Kim, D.; Lee, N.; Park, M.; Kim, B. H.; An, K.; Hyeon, T., Synthesis of uniform ferrimagnetic magnetite nanocubes. J. Am. Chem. Soc. 2008, 131, 454-455.
8 Peng, S.; Sun, S., Synthesis and Characterization of Monodisperse Hollow Fe_3O_4 Nanoparticles. Angew. Chem. Int. Ed. 2007, 119, 4233-4236.
9 Li, Z.; Tan, B.; Allix, M.; Cooper, A. I.; Rosseinsky, M. J., Direct coprecipitation route to monodisperse dual-functionalized magnetic iron oxide nanocrystals without size selection. Small 2008, 4 , 231-239.
10 Sun, S.; Zeng, H., Size-controlled synthesis of magnetite nanoparticles. J. Am. Chem. Soc. 2002, 124, 8204-8205.
11 Mathur, S.; Barth, S.; Werner, U.; Hernandez-Ramirez, F.; Romano-Rodriguez, A., Chemical Vapor Growth of One-dimensional Magnetite Nanostructures. Adv. Mater. 2008, 20, 1550-1554.
12 Deng, H.; Li, X.; Peng, Q.; Wang, X.; Chen, J.; Li, Y., Monodisperse magnetic single-crystal ferrite microspheres. Angew. Chem. Int. Ed. 2005, 44, 2782-2785.
13 Liu, J.; Sun, Z.; Deng, Y.; Zou, Y.; Li, C.; Guo, X.; Xiong, L.; Gao, Y.; Li, F.; Zhao, D., Highly water-dispersible biocompatible magnetite particles with low cytotoxicity stabilized by citrate groups. Angew. Chem. Int. Ed. 2009, 48, 5875-5879.
14 Gao, J.; Ran, X.; Shi, C.; Cheng, H.; Cheng, T.; Su, Y., One-step solvothermal synthesis of highly water-soluble, negatively charged superparamagnetic Fe_3O_4 colloidal nanocrystal clusters. Nanoscale 2013, 5, 7026-7033.
15 Wang, L.; Tang, S.; Zhou, H., Controlled Synthesis of Magnetic Iron Oxide Nanoparticles Within a Supramolecular Organogel Fiber Network. Sci. Adv. Mater. 2013, 5, 822-829.
16 Kovalenko, M. V.; Bodnarchuk, M. I.; Lechner, R. T.; Hesser, G.; Schäffler, F.; Heiss, W., Fatty acid salts as stabilizers in size-and shape-controlled nanocrystal synthesis: the case of inverse spinel iron oxide. J. Am. Chem. Soc. 2007, 129, 6352-6353.
17 Yang, C.; Wu, J.; Hou, Y., Fe_3O_4 nanostructures: synthesis, growth mechanism, properties and applications. Chem. Commun. 2011, 47, 5130-5141.
18 Dupont, J., From molten salts to ionic liquids: A "nano" journey. Acc. Chem. Res. 2011, 44, 1223-1231.
19 Tang, S.; Baker, G. A.; Zhao, H., Ether- and alcohol-functionalized task-specific ionic liquids: attractive properties and applications. Chem Soc Rev 2012, 41, 4030-4066.
20 Recham, N.; Dupont, L.; Courty, M.; Djellab, K.; Larcher, D.; Armand, M.; Tarascon, J. M., Ionothermal synthesis of tailor-made $LiFePO_4$ powders for Li-ion battery applications. Chem. Mater. 2009, 21, 1096-1107.
21 Lian, J.; Duan, X.; Ma, J.; Peng, P.; Kim, T.; Zheng, W., Hematite (α-Fe_2O_3) with various morphologies: ionic liquid-assisted synthesis, formation mechanism, and properties. ACS nano 2009, 3, 3749-3761.
22 Zheng, W.; Liu, X.; Yan, Z.; Zhu, L., Ionic liquid-assisted synthesis of large-scale TiO_2 nanoparticles with controllable phase by hydrolysis of $TiCl_4$. ACS nano 2008, 3, 115-122.
23 Duan, X.; Kim, T.; Li, D.; Ma, J.; Zheng, W., Understanding the effect models of ionic liquids in the synthesis of NH_4-Dw and gamma-AlOOH nanostructures and their conversion into porous gamma-Al_2O_3. Chem. Eur. J. 2013, 19, 5924-5937.
24 Zhang, J.; Wang, J.; Zhou, S.; Duan, K.; Feng, B.; Weng, J.; Tang, H.; Wu, P., Ionic liquid-controlled synthesis of ZnO microspheres. J. Mater. Chem. 2010, 20, 9798-9804.
25 Liu, X.; Duan, X.; Qin, Q.; Wang, Q.; Zheng, W., Ionic liquid-assisted solvothermal synthesis of oriented self-assembled Fe_3O_4 nanoparticles into monodisperse nanoflakes. CrystEngComm 2013, 15, 3284-3287.
26 Zeng, Y.; Hao, R.; Xing, B.; Hou, Y.; Xu, Z., One-pot synthesis of Fe_3O_4 nanoprisms with controlled electrochemical properties. Chem. Commun. 2010, 46, 3920-3922.
27 Jacobi, H. W.; Annor, T.; Quansah, E., Investigation of the photochemical decomposition of nitrate, hydrogen peroxide, and formaldehyde in artificial snow. J. Photoch. Photobio. A. 2006, 179, 330-338.
28 Uchida, M.; Kikuchi, K.; Okuwaki, A., Decomposition of NO_3^- by lead pellets with wet ball milling. Waste Manage. 1999, 19, 213-219.

29 Uchida, M.; Okuwaki, A., Decomposition of nitrate by in situ buff abrasion of lead plate. Hydrometallurgy 1998, 49, 297-308.
30 Lin, M.; Huang, H.; Liu, Z.; Liu, Y.; Ge, J.; Fang, Y., Growth-Dissolution-Regrowth Transitions of Fe_3O_4 Nanoparticles as Building Blocks for 3D Magnetic Nanoparticle Clusters under Hydrothermal Conditions. Langmuir 2013, 29, 15433-15441.
31 Narayanaswamy, A.; Xu, H.; Pradhan, N.; Kim, M.; Peng, X., Formation of nearly monodisperse In_2O_3 nanodots and oriented-attached nanoflowers: hydrolysis and alcoholysis vs pyrolysis. J. Am. Chem. Soc. 2006, 128, 10310-10319.
32 Narayanaswamy, A.; Xu, H.; Pradhan, N.; Peng, X., Crystalline nanoflowers with different chemical compositions and physical properties grown by limited ligand protection. Angew. Chem. Int. Ed. 2006, 45, 5361-5364
33 Whittington, C. L.; Maza, W. A.; Woodcock, H. L.; Larsen, R. W., Understanding ion sensing in Zn(II) porphyrins: spectroscopic and computational studies of nitrite/nitrate binding. Inorg. Chem. 2012, 51, 4756-4762.
34 Lee, J. W.; Kim, E. A.; Kim, Y. J.; Lee, Y. A.; Pak, Y.; Jung, O. S., Relationship between the Ratio of Ligand to Metal and the Coordinating Ability of Anions. Synthesis and Structural Properties of AgX-Bearing Bis (4-pyridyl) dimethylsilane (X-= NO_2^-, NO_3^-, $CF3SO_3^-$, and PF_6^-). Inorg. Chem. 2005, 44, 3151-3155.
35 Cornell, R. M.; Schwertmann, U., The iron oxides: structure, properties, reactions, occurrences and uses, WILEY-VCH, Weinheim, 2003.
36 Dong, K.; Zhang, S.; Wang, D.; Yao, X., Hydrogen bonds in imidazolium ionic liquids. J. Phys. Chem. A. 2006, 110, 9775-9782.
37 Minella M, Marchetti G, De Laurentiis E, et al. Photo-Fenton oxidation of phenol with magnetite as iron source. Applied Catalysis B: Environmental. 2014, 154, 102-109.